

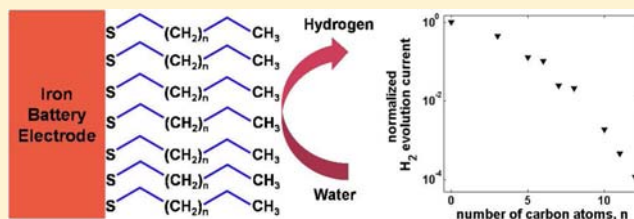
# Self-Assembled Monolayers of *n*-Alkanethiols Suppress Hydrogen Evolution and Increase the Efficiency of Rechargeable Iron Battery Electrodes

Souradip Malkhandi, Bo Yang, Aswin K. Manohar, G. K. Surya Prakash, and S. R. Narayanan\*

Loker Hydrocarbon Research Institute, Department of Chemistry, University of Southern California, Los Angeles, California 90089, United States

## Supporting Information

**ABSTRACT:** Iron-based rechargeable batteries, because of their low cost, eco-friendliness, and durability, are extremely attractive for large-scale energy storage. A principal challenge in the deployment of these batteries is their relatively low electrical efficiency. The low efficiency is due to parasitic hydrogen evolution that occurs on the iron electrode during charging and idle stand. In this study, we demonstrate for the first time that linear alkanethiols are very effective in suppressing hydrogen evolution on alkaline iron battery electrodes. The alkanethiols form self-assembled monolayers on the iron electrodes. The degree of suppression of hydrogen evolution by the alkanethiols was found to be greater than 90%, and the effectiveness of the alkanethiol increased with the chain length. Through steady-state potentiostatic polarization studies and impedance measurements on high-purity iron disk electrodes, we show that the self-assembly of alkanethiols suppressed the parasitic reaction by reducing the interfacial area available for the electrochemical reaction. We have modeled the effect of chain length of the alkanethiol on the surface coverage, charge-transfer resistance, and double-layer capacitance of the interface using a simple model that also yields a value for the interchain interaction energy. We have verified the improvement in charging efficiency resulting from the use of the alkanethiols in practical rechargeable iron battery electrodes. The results of battery tests indicate that alkanethiols yield among the highest faradaic efficiencies reported for the rechargeable iron electrodes, enabling the prospect of a large-scale energy storage solution based on low-cost iron-based rechargeable batteries.



## INTRODUCTION

The prime motivation for this study is the potential of iron-based aqueous rechargeable batteries as a transformational solution for large-scale battery-based energy storage. The low cost of iron, the robustness of the iron electrode to repeated charge and discharge cycles, combined with the global abundance and eco-friendliness of iron are particularly attractive for a large-scale energy storage system. Such energy storage systems are direly needed for the integration of renewable energy generation into the electricity grid.<sup>1</sup> However, the principal limitation to the exploitation of the iron electrode in aqueous alkaline media has been the parasitic evolution of hydrogen that occurs during battery charging and idle stand.<sup>2</sup> The hydrogen evolution process reduces the charging efficiency and thus the overall electrical energy efficiency of the battery; almost 50% of the energy is wasted during charging. Thus, the suppression of hydrogen evolution will have a transformational impact on the commercial deployment of iron-based batteries. Specifically, suppressing hydrogen evolution will (1) enhance the round-trip energy efficiency, (2) reduce the size of the battery, and (3) reduce the loss of water from the battery during charging.

Recently, we reported the benefits of in situ electro-deposition of bismuth on iron in suppressing the evolution of

hydrogen.<sup>3</sup> However, the incorporation of bismuth additives in the iron electrode, albeit in small quantities, can impact the cost and the ability to recycle iron electrodes. Therefore, in the present study, we identify the benefit of using organo-sulfur compounds to improve the performance of iron electrodes. Specifically, we find that *n*-alkanethiols are particularly effective in suppressing the hydrogen evolution reaction on the iron electrode in alkaline media. These additives will be required only in very small quantities (ng/cm<sup>2</sup> of the battery electrode). Thus, we do not anticipate any negative impacts on the cost and environmental friendliness of iron-based batteries resulting from the use of organo-sulfur compounds.

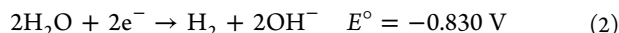
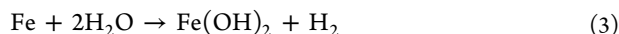
The evolution of hydrogen at an iron battery electrode during charging and idle stand is because the standard reduction potential of the iron electrode reaction is negative to that of the hydrogen evolution reaction (eqs 1–3).

**Charging Process at the Iron Electrode. Useful Battery Electrode Reaction.**



Received: September 26, 2012

Published: December 13, 2012

*Parasitic Hydrogen Evolution.***Wasteful Self-Discharge during “Idle Stand” of Electrode.**

We may conclude from eqs 2 and 3, that suppression of the hydrogen evolution reaction can be achieved by excluding water from the surface of the iron electrode, since water is a reactant in the wasteful hydrogen-generating reactions. Alkanethiols and other organo-sulfur compounds are known to form self-assembled monolayers on various metal surfaces through the interaction of the sulfur atom of the thiol with the metal.<sup>4</sup> Such self-assembled layers are generally compact and hydrophobic and can reduce substantially the access of reactants to the electrode–solution interface. Therefore, we can expect such self-assembled monolayers of alkanethiols on an iron surface to inhibit the hydrogen evolution reaction.

We found several reports on the effectiveness of thiols and other compounds in suppressing the corrosion of copper in aerated acidic solutions.<sup>5</sup> In alkaline media, the alkanethiols are in the ionized “thiolate” form but are still capable of forming self-assembled monolayers. However, there has been no report of studies on the effect of such compounds on iron in alkaline media or in rechargeable batteries. Since the properties of self-assembled monolayers depend on chain length of the alkanethiol,<sup>6</sup> we expected the degree of suppression of the hydrogen evolution reaction to depend on the molecular structure of the alkanethiol. We also recognized that, if the self-assembled layer was too compact, then the total exclusion of water from the surface will inhibit all the electrochemical processes including the desirable process of charging the battery electrode (eq 1). Therefore, it was important to identify the chain length of alkanethiol that achieved optimal inhibition without complete blockage of all the surface reactions. Another important aspect of exploiting this type of self-assembly was the selectivity of formation of such self-assembled monolayers only on the bare surface of iron and not on surfaces covered with oxides or hydroxides.<sup>5h</sup> Consequently, as iron hydroxide is converted to iron in the charging process (eq 1), the adsorption of the alkanethiols can cover the newly generated iron surface and ensure a steady level of suppression of hydrogen evolution throughout the charge process.

In this report, we address three scientific questions: (1) To what extent do the self-assembled layers of alkanethiols suppress the hydrogen evolution reaction during charging of the iron electrode? (2) How does the molecular structure of the alkanethiol influence the extent of suppression of hydrogen evolution? (3) What is the minimum alkane chain length that achieves adequate hydrogen suppression without impairing the battery discharge process?

**EXPERIMENTAL SECTION**

Three types of experiments were conducted to study the effect of alkanethiols: (1) steady-state potentiostatic polarization experiments on polished iron disk electrodes, (2) electrochemical impedance spectroscopy of polished iron disk electrodes, and (3) measurement of the faradaic efficiency of charging of porous iron electrodes prepared with high-purity carbonyl iron.<sup>3</sup> The potentiostatic polarization and impedance measurements were conducted on a high-purity iron disk (99.999%, 5 mm diameter, Alfa–Aesar) mounted on a rotating-disk electrode (Pine Instruments, change-disk electrode AFESTQ050). The disks were polished with 0.05  $\mu\text{m}$  alumina and cleaned with

isopropanol and acetone before each experiment. Experiments were conducted in an electrochemical cell made of polyfluoroethylene that contained the following: 1 M potassium hydroxide solution (purged with argon gas) as the electrolyte, a platinum wire counter electrode, and a mercury–mercuric oxide (MMO) reference electrode (20% potassium hydroxide,  $E^\circ = +0.098 \text{ V}$ ). Unless otherwise mentioned, all values of electrode potential are reported versus the MMO reference electrode. The electrochemical cell was thoroughly cleaned prior to each experiment to avoid cross-contamination by the alkanethiols.

Steady-state polarization measurements in the potential range  $-0.85$  to  $-1.3 \text{ V}$  versus the MMO reference electrode were conducted by stepping the electrode potential 50 mV at a time and holding the potential for 300 s before recording the steady-state current (Ametek-PAR-VMC-4 potentiostat/galvanostat/frequency response analyzer). Electrochemical impedance was measured as a function of electrode potential with a sinusoidal-excitation signal of 2 mV (peak-to-peak) over the frequency range 50 mHz to 100 kHz. The polarization and impedance experiments were repeated with 1 M potassium hydroxide solution containing 10 mM linear alkanethiols of the general formula  $\text{C}_n\text{H}_{(2n-1)}\text{SH}$  and  $n$  values of 3, 4, 5, 6, 7, 8, 10, 11, and 12 (Sigma–Aldrich). The electrodes were equilibrated in the alkanethiol-containing electrolyte for 60 min under argon atmosphere prior to the electrochemical measurements. The period of 60 min was adequate to achieve equilibration as indicated by steady-state currents (see the Supporting Information, Figure S1).

**RESULTS AND DISCUSSION**

**Suppression of Hydrogen Evolution Reaction.** Results of the polarization measurements on the iron disk electrode are shown in Figure 1.

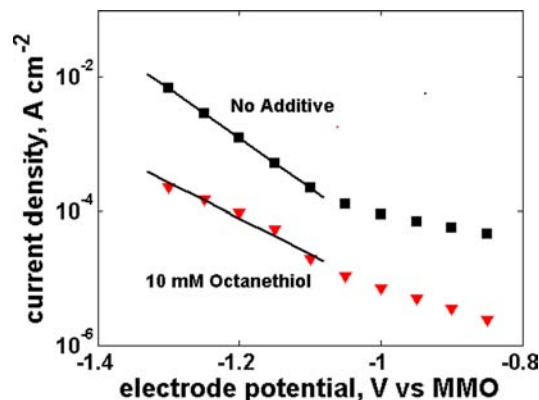


**Figure 1.** Steady-state potentiostatic polarization of rotating iron disk in 1 M potassium hydroxide with and without 10 mM octanethiol.

In the absence of any alkanethiol additive, the cathodic current for hydrogen evolution on iron was significant at values more negative to  $-0.95 \text{ V}$ . In the potential range  $-1.050$  to  $-1.300 \text{ V}$ , the Tafel slope and exchange current density for hydrogen evolution were 134 mV/decade and  $1.1 \times 10^{-5} \text{ A/cm}^2$ , respectively. These values were in general agreement with those reported in the literature.<sup>7</sup> In a solution of 1 M potassium hydroxide containing 10 mM *n*-octanethiol, the Tafel slope was 184 mV/decade, and the exchange current density was  $2.7 \times 10^{-6} \text{ A/cm}^2$ .

The increase in the value of the Tafel slope with the addition of *n*-octanethiol suggested that the electron transfer process for hydrogen evolution was hindered in the presence of the thiol. We can expect the double-layer structure to be considerably altered by the high surface coverage of the thiol layer which in turn would cause the interfacial electric field gradient to be more distributed for a thiol-covered electrode. Such a

distributed interfacial potential drop would necessitate a higher value of overpotential to effect the same increase in current (manifesting as a higher Tafel slope). Similar high values of Tafel slopes have been observed with the specific adsorption of chromate on iron in alkaline media.<sup>7b</sup> The reduced values of exchange current density were attributed to a reduced area available for reaction following the adsorption of the *n*-octanethiol. Based on the values of exchange current density, the surface coverage of the *n*-octanethiol was estimated to be approximately 75%.

Impedance spectroscopy measurements with and without *n*-octanethiol confirmed the conclusions from the steady-state polarization measurements and led to additional insights into the self-assembly of *n*-octanethiol. The results of impedance spectroscopy (Figure 2a) were fitted to a simple electrical equivalent circuit (Figure 2b) with the following elements: (a) capacitance,  $C_{dl}$ , associated with the double layer at the electrode–electrolyte interface; (b) resistance,  $R_{ct}$ , associated with the charge-transfer process; and (c) resistance,  $R_{\Omega}$ , associated with the Ohmic resistance of the electrode and electrolyte. The Warburg impedance element was not included in the equivalent circuit because limitations from mass transport of water or hydroxide ions were not expected to make a significant contribution to the impedance in the range of potentials studied. The standard error in the fitted parameter was less than 5% without the thiol. For the case with thiol, the standard error ranged from 10% to 25% (see the Supporting Information, Figure S2a–f for fitted data). Although we could have achieved less than 5% with the use of a constant phase element (CPE) instead of the capacitance, we chose not to because of the lack of a convincing physical equivalent of the CPE for the interface.

The charge-transfer resistance (Figure 2a) increased with the addition of *n*-octanethiol, and this was consistent with the results from steady-state polarization measurements (Figure 1). As before, we conclude that the adsorption of *n*-octanethiol decreases the available surface area for the hydrogen evolution reaction and thus increases the observed value of charge-transfer resistance. Therefore, the surface coverage by *n*-octanethiol can be determined from the increase in the value of charge-transfer resistance at any particular potential.<sup>8</sup>

The double-layer capacitance in the range  $-0.85$  to  $-0.90$  V was about the same with and without *n*-octanethiol. However, at more negative potentials, in the range  $-1.00$  to  $-1.30$  V, the double-layer capacitance (Figure 2d) decreased markedly in the presence of *n*-octanethiol. This decrease may be understood in terms of the faradaic conversion of iron hydroxide to iron occurring on the surface. In the potential region  $-0.85$  to  $-1.0$  V, the iron electrode is largely covered by an iron hydroxide film. At negative potentials less than  $-1.0$  V, the iron hydroxide is reduced to elemental iron, and thus, more sites become available for the adsorption of *n*-octanethiol. Consequently, the progressive adsorption and self-assembly of *n*-octanethiol results in a decrease in the double-layer capacitance (Figure 2d). Also, at  $-1.3$  V, the self-assembly of *n*-octanethiol molecules is complete, and the exclusion of water occurs from the surface of the iron electrode. Thus, the adsorption of *n*-octanethiol to form a compact layer leads to a very low value of double-layer capacitance. These observations also confirm that the adsorption of the *n*-alkanethiols occurs preferentially on iron although iron hydroxide may be present. The slight increase in capacitance between  $-1.2$  and  $-1.3$  V in the absence of the thiol could be due to the variations in area that

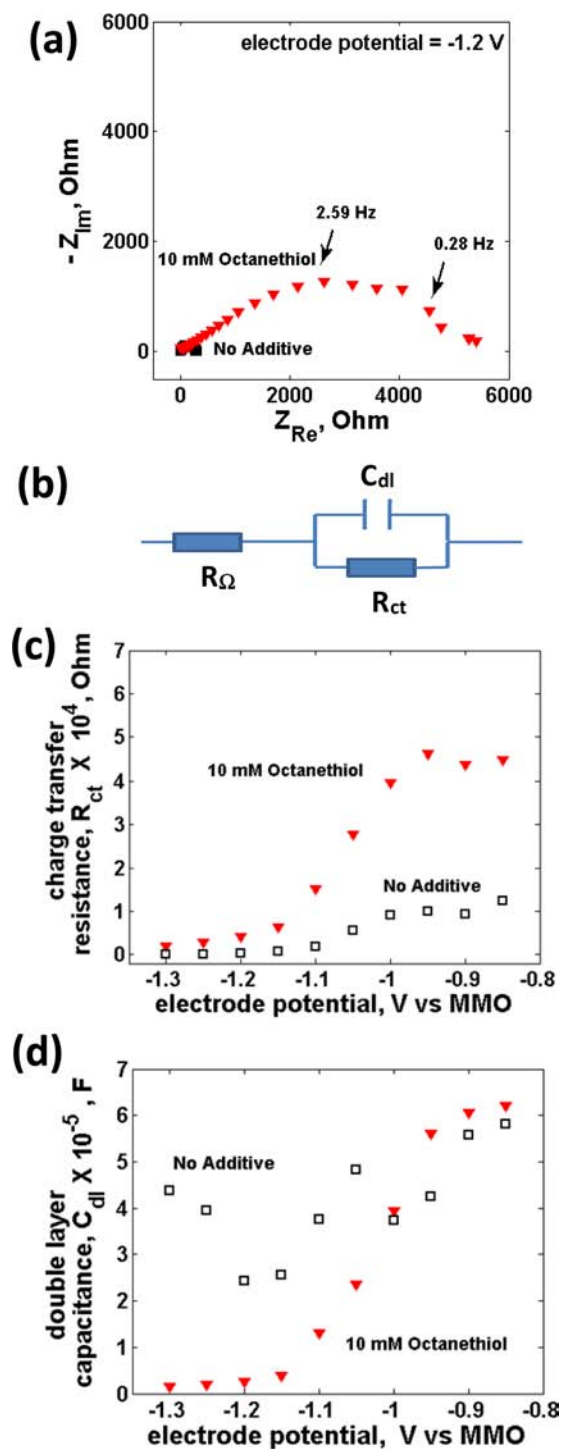


**Figure 2.** Representative impedance data of the iron disk electrode in 1 M potassium hydroxide (a) at electrode potential of  $-1.05$  V in the absence and presence of 10 mM octanethiol; (b) equivalent circuit used for analysis; (c) variation of charge-transfer resistance with potential; (d) variation of double-layer capacitance with electrode potential.

accompany the reduction of the surface iron oxides at these potentials.

**Dependence of Chain Length of *n*-Alkanethiol on Charge-Transfer Resistance and Double-Layer Capacitance.** The current for hydrogen evolution, measured by steady-state polarization measurements, depended strongly on

the chain length of the *n*-alkanethiol. The relative hydrogen evolution rate was calculated by normalizing the hydrogen evolution current observed with the alkanethiol to that observed in the absence of the alkanethiol. This type of normalization removed the variability originating from the surface roughness of the iron disks and permitted a valid comparison of results from different iron disk electrodes. For the chain length of *n* = 12, the rate of hydrogen evolution was reduced by 4 orders of magnitude (Figure 3a).

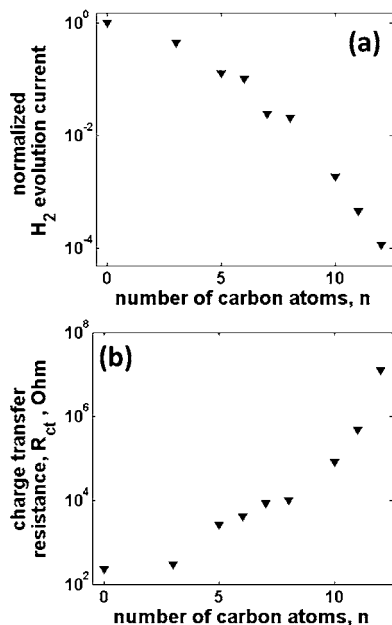


**Figure 3.** (a) Dependence of the normalized hydrogen evolution current at  $-1.20$  V vs MMO on the chain length of alkanethiol (from potentiostatic polarization measurements); (b) dependence of charge-transfer resistance at  $-1.20$  V vs the MMO on the chain length of alkanethiol (impedance measurements).

The logarithmic dependence of the hydrogen evolution rate and charge-transfer resistance on the chain length of the alkanethiol may be understood in terms of the interactions of the alkanethiols with the iron surface and the van der Waals interactions between the alkanethiol chains. The interaction of the thiol with the iron surface occurs through chemisorption of the thiol end-group. The molar free energy change for the interaction of the thiol end-group with the iron surface is primarily dependent on the electron affinity of the sulfur center and is largely independent of the chain length. However, the compactness of the self-assembled layers would be dependent on the lateral interactions between the alkanethiol chains. The strength of such interchain interactions is dependent on the length of the chains.<sup>61</sup> Therefore, we may represent the molar free energy change for the formation of self-assembled monolayers to be a sum of a constant value associated with the interactions of the sulfur head with the iron surface and a variable value that increases with chain length as expressed in eq 4.

These results confirmed that the surface coverage and compactness of the self-assembled layer formed by the alkanethiols depended significantly on the chain length. Thus, the desired degree of suppression of hydrogen evolution may be achieved by the appropriate choice of chain length. For example, to realize a 95% reduction in hydrogen evolution rate

on iron, the *n* value for the alkanethiol must be chosen in the range *n* = 6–8. The charge transfer resistance determined from impedance measurements also increased by several orders of magnitude over the range of *n* = 3–12 (Figure 3b).

$$\Delta G_{\text{SAM}} = \Delta G_{\text{Sulfur-Fe}} + n \frac{\Delta(\Delta G_{\text{interchain}})}{\Delta n} \quad (4)$$

In eq 4,  $\Delta G_{\text{SAM}}$  is the molar free energy change for the formation of the self-assembled monolayer,  $\Delta G_{\text{Sulfur-Fe}}$  is the molar free energy change arising from the sulfur–iron bond,  $\Delta G_{\text{interchain}}$  is the molar free energy change for the interchain interaction, and *n* is the value of the carbon atoms in the alkanethiol.<sup>6h</sup>

The molar free energy change is also related to the equilibrium constant for the adsorption–desorption process by the relationship of basic chemical thermodynamics:

$$\Delta G_{\text{SAM}} = \Delta G_{\text{SAM}}^0 + RT \ln K_{\text{eq}} \quad (5)$$

In eq 5,  $\Delta G_{\text{SAM}}^0$  is the standard molar free energy for the formation of the self-assembled monolayer,  $K_{\text{eq}}$  is the equilibrium constant for the adsorption–desorption process, *R* is the gas constant, and *T* is the absolute temperature.

The equilibrium surface coverage may be related to the equilibrium constant and the activity of the thiol as follows:

$$\{\theta/(1 - \theta)\} = K_{\text{eq}} a_{\text{thiol}}^* \quad (6)$$

where  $\theta$  is the fraction of the surface covered by the alkanethiol and  $a_{\text{thiol}}^*$  is the activity of the adsorbing species in solution.

Combining eqs 4–6 we have

$$\begin{aligned} \ln\{\theta/(1 - \theta)\} &= (1/RT)\{(\ln a_{\text{thiol}}^*) \\ &+ (\Delta G_{\text{Sulfur-Fe}} - \Delta G_{\text{SAM}}^0)\} \\ &+ n\{(\Delta(\Delta G_{\text{interchain}})/\Delta n)\}/RT \quad (7) \end{aligned}$$

The relationship in eq 7 is similar to the Langmuir–Frumkin isotherm that includes lateral interactions between adsorbate molecules. Since the faradaic reaction occurs only on the areas not covered by the alkanethiol, the observed value of charge-transfer resistance is related to the surface coverage of the alkanethiol,  $\theta$ , by

$$(R_{\text{ct-thiol}}/R_{\text{ct-0}})(S_0/S_{\text{thiol}}) = 1/(1 - \theta) \quad (8)$$

where  $R_{\text{ct-0}}$  and  $R_{\text{ct-thiol}}$  are the charge-transfer resistances in the absence and presence of the additive, respectively, and  $S_0$  and  $S_{\text{thiol}}$  are the corresponding Tafel slopes.

A plot of  $\ln\{\theta/(1 - \theta)\}$  versus the chain length *n* (Figure 4) gave a straight line. The value of  $\Delta(\Delta G_{\text{interchain}})/\Delta n$  was calculated from the slope to be  $2.6 \text{ kJ mol}^{-1}$  per carbon atom. Since van der Waals' forces govern such lateral interactions that lead to self-assembly, we compared the molar free energy of interchain interaction determined here with that of the molar free energy of fusion of alkanes. We find that the value of molar free energy of fusion for long-chain alkanes of  $3.1 \text{ kJ mol}^{-1}$  per carbon is about the same magnitude as the molar free energy for interchain interaction of the alkyl groups in the self-assembled alkanethiols.<sup>9</sup> The agreement of the values for interchain interaction derived from the analysis of the alkanethiol adsorption on iron with experimental values from the fusion of alkanes strongly supports our overall understanding of the suppression of hydrogen evolution by self-assembly of the alkanethiols on the iron sites.

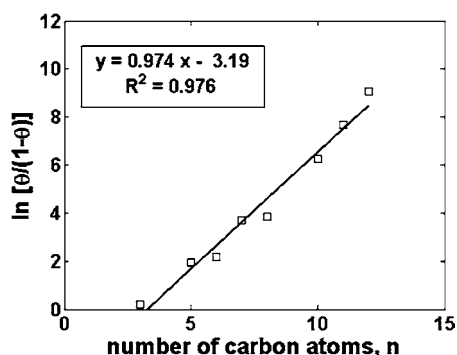


Figure 4. Dependence of the coverage function  $\ln(\theta/(1-\theta))$  on the number of carbon atoms in the alkanethiol.

The impedance measurements in the range  $-1.0$  to  $-1.3$  V also indicated that the chain length of the alkanethiol had a marked influence on the double-layer capacitance (Figure 5).

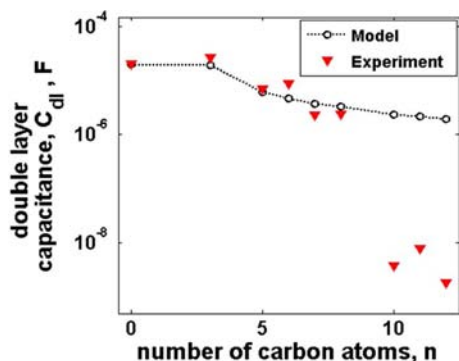


Figure 5. Influence of the  $n$  value of the alkanethiol  $C_nH_{n-1}SH$  on the double-layer capacitance of the iron disk electrode in 1 M potassium hydroxide at  $-1.2$  V vs the MMO.

The decrease in double-layer capacitance with the increasing chain length of the alkanethiol can be understood in terms of the same adsorption model used to explain the charge-transfer resistance. The double-layer capacitance may be modeled by adding the contributions from the covered and uncovered areas of the electrode and expressed as

$$C_{\text{obs}} = Af\{\theta C_{\text{cov}} + (1 - \theta)C_{\text{uncov}}\} \quad (9)$$

where  $C_{\text{obs}}$  is the observed value of double-layer capacitance,  $C_{\text{cov}}$  and  $C_{\text{uncov}}$  are specific capacitance values for the covered and uncovered areas, respectively,  $\theta$  is the coverage of the surface by the thiols with  $0 < \theta < 1$ ,  $A$  is the geometric area, and  $f$  is the roughness factor.

As before, since only uncovered areas can sustain a faradaic reaction, the charge-transfer resistance of the interface can be used to determine  $\theta$  (eq 8).  $C_{\text{cov}}$  is modeled as a parallel-plate capacitor with the self-assembled monolayers forming a dielectric layer of thickness equal to the chain length of the alkanethiol and thus

$$C_{\text{cov}} = \epsilon \epsilon_0 / (d_{\text{thiol}}) \quad (10)$$

where  $\epsilon$  is the dielectric constant of the layer,  $\epsilon_0$  is the permittivity of free space, and  $d_{\text{thiol}}$  is length of the alkanethiol molecule. The length of the alkanethiol in centimeters is expressed in terms of the number of carbon atoms by the following relationship:<sup>6g</sup>

$$d_{\text{thiol}}, \text{ cm} = 0.5 \times 10^{-8} + n(1.24 \times 10^{-8}) \quad (11)$$

$C_{\text{uncov}}$  is the double-layer capacitance of the film-free interface obtained from measurements without alkanethiol.

Therefore, from eqs 9–11,

$$C_{\text{obs}} = Af\{\theta \epsilon \epsilon_0 / [0.5 \times 10^{-8} + n(1.24 \times 10^{-8})] + (1 - \theta)C_{\text{uncov}}\} \quad (12)$$

Using eq 12, we have calculated the value of double-layer capacitance for alkanethiols of different values of chain length using the following values:<sup>10</sup>  $A = 0.196 \text{ cm}^2$ ;  $f = 8$ ;  $\epsilon = 2.16$ ;  $\epsilon_0 = 8.85 \times 10^{-12} \text{ C}^2 \text{ N}^{-1} \text{ m}^{-2}$ ; and  $C_{\text{uncov}}$  ranged from 10.2 to 34.8  $\mu\text{F}/\text{cm}^2$ . Values of  $\theta$  were derived from eq 8.

As shown in Figure 5, the double-layer capacitance predicted by the model is in good agreement with the experimental values up to a chain length of  $n = 8$ . However, for  $n = 10$ – $12$ , the experimental values of capacitance are lower than those predicted by the model. Factors that could reduce the value of double-layer capacitance at higher values of chain length are (1) the reduction in the value of the dielectric constant of the films with increasing chain length, (2) the degree of compactness of the self-assembled layers, and (3) the formation of multilayer films. These factors are not included in the simple model presented here. Also, in an effort to use only measurable quantities in the model, we have avoided invoking any arbitrary parameters. Despite these simplifications, the model does predict the properties of the adsorbed films formed up to a chain length of eight.

**Performance of Battery Electrodes with  $n$ -Alkanethiol.** Results of steady-state polarization measurements on high-purity iron disks (Figure 3) suggest that  $n$ -hexanethiol ( $n = 6$ ) reduces the hydrogen evolution rate at the iron electrode by about 90%. Therefore, we decided to test the properties of  $n$ -hexanethiol on iron battery electrodes as an example of the  $n$ -alkaneithiol. Such a battery electrode was prepared from high-purity carbonyl iron powder. In a recent study, we have demonstrated a high-performance iron electrode of this type for large-scale energy storage.<sup>3</sup> Such iron electrodes were coated with  $n$ -hexanethiol by immersing in an ethanolic solution of  $n$ -hexanethiol followed by drying in a stream of argon (to avoid oxidation of the  $n$ -hexanethiol). The iron electrodes coated with  $n$ -hexanethiol were then charged and discharged several times until a stable capacity was achieved. Then, the iron electrode was subjected to further charge/discharge cycling for at least 25 cycles during which the rate of evolution of hydrogen during the charging process and the charging efficiency was determined; the capacity realized in the discharge step and the amount of charge used in charging were determined to calculate the efficiency.

With  $n$ -hexanethiol on the porous carbonyl iron electrode, the rate of evolution of hydrogen was reduced by at least 30% (Figure 6a) compared to the electrode without  $n$ -hexanethiol. Such a reduction is quite significant from an overall efficiency standpoint. The reduced rate of evolution of hydrogen and the high charging efficiency were retained over at least 25 cycles (Figure 6b), suggesting that the function of the alkanethiol layers was retained on the surface of the iron electrode even after many charge/discharge cycles.

The enhanced charging efficiency observed with the coating of  $n$ -hexanethiol was consistent with the suppression of hydrogen evolution and the increase in charge-transfer resistance observed on the iron disk electrodes. While the

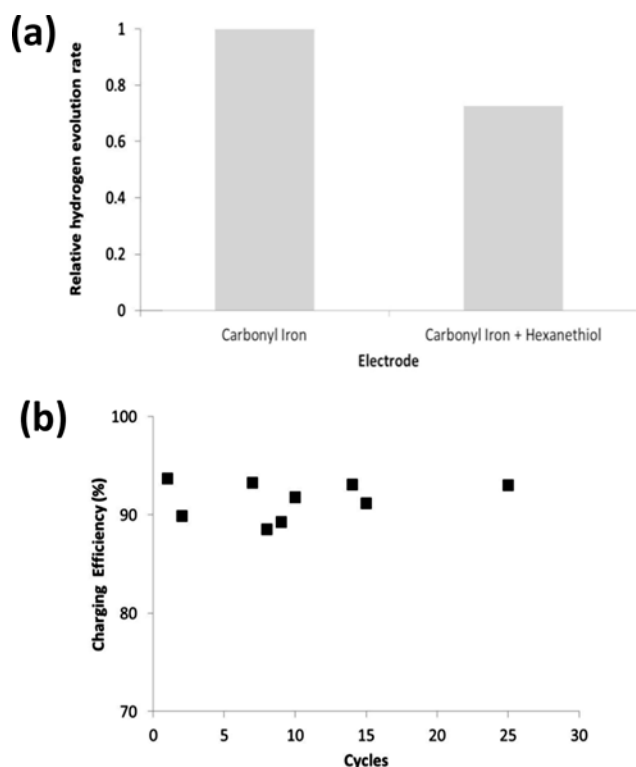


**Figure 6.** Faradaic efficiency measurements: (a) relative rates of hydrogen evolution on carbonyl electrodes with and without hexanethiol; (b) charging efficiency of a carbonyl iron electrode with hexanethiol as a function of cycling at 200 mA charge and 20 mA discharge (capacity of 0.3 Ah).

iron disks showed about 90% suppression, the porous electrodes showed only a 30% reduction. We believe that some of this lower level of suppression can be attributed to the differences in distribution of alkanethiol in a porous battery electrode versus the flat disk electrode used in the electrochemical studies. Further, all the fundamental studies were performed without exposure to air, whereas the battery electrode cycling tests were conducted with free access to air that will cause loss of the thiol by air oxidation. The relatively stable performance over 25 cycles (obtained over a period of a month) suggested that the beneficial effect of the thiol can be retained even when dissolved oxygen is present in the cell. The migration of the thiol across the cell is not expected to affect the performance of the air electrode as the thiol will be oxidized to soluble sulfonates.<sup>11</sup> Regardless of these differences, the carbonyl iron electrode with *n*-hexanethiol had a charging efficiency of about 92% which is a 5-fold reduction in hydrogen evolution rate over the commercial electrodes in which the charging efficiency is 55–70%. Thus, the charging efficiency of the alkanethiol-coated iron electrodes was among the highest observed with rechargeable iron electrodes and compared well with the electrodes containing bismuth sulfide additives developed by us recently.<sup>3</sup>

## CONCLUSIONS

Our study shows that self-assembled monolayers of alkanethiols can substantially reduce the rate of hydrogen evolution on iron in alkaline media and thereby mitigate the problem of low charging efficiency of the rechargeable iron electrode. Electrochemical measurements confirm that the degree of suppression

of hydrogen evolution is determined by the differences in the extent of coverage of the surface by the alkanethiol molecules. The chain length of the alkanethiol was found to markedly influence the rate of hydrogen evolution. For a chain length of  $n \geq 6$ , greater than 90% reduction in hydrogen evolution rate was observed. The dependence of the charge-transfer resistance and the double-layer capacitance on the chain length of the alkanethiol have been modeled with a Langmuir–Frumkin type isotherm. The analysis showed that the difference in surface coverage was caused by increased interchain interactions of alkanethiol molecules with higher chain length. The energy of interchain interactions was estimated to be about  $2.6 \text{ kJ mol}^{-1}$  per carbon atom and found to be of the same magnitude as the molar free energy of fusion of long-chain alkanes per carbon atom, confirming that van der Waals' interactions between the thiol chains determine the surface coverage by the alkanethiols. The model proposed here could predict the experimental values of double-layer capacitance very well up to a chain length of  $n = 8$ . The benefits of alkanethiols in suppressing hydrogen evolution was confirmed with practical iron rechargeable battery electrodes coated with *n*-hexanethiol, wherein the high charging efficiency and suppression of hydrogen evolution was retained over multiple charge/discharge cycles. The research presented here demonstrates a new and promising approach of exploiting self-assembled monolayers for improving the charging efficiency of rechargeable iron batteries and rendering these inexpensive batteries attractive for large-scale energy storage.

## ASSOCIATED CONTENT

### Supporting Information

Data on the time required for equilibration of the self-assembled layers and also examples of the fitting of the impedance data. This material is available free of charge via the Internet at <http://pubs.acs.org>.

## AUTHOR INFORMATION

### Corresponding Author

sri.narayan@usc.edu

### Notes

The authors declare no competing financial interest.

## ACKNOWLEDGMENTS

The research reported here was supported by the U.S. Department of Energy ARPA-E (GRIDS program, DE-AR0000136), the Loker Hydrocarbon Research Institute, and the University of Southern California.

## REFERENCES

- (1) Narayanan, S. R.; Prakash, G. K.; Manohar, A.; Yang, B.; Malkhandi, S. *Solid State Ionics* **2012**, *216*, 105.
- (2) (a) Falk, S. U.; Salkind, A. J. *Alkaline Storage Batteries*; John Wiley: New York, 1969. (b) Vijayamohan, K.; Shukla, A. K.; Sathyanarayana, S. J. *Electroanal. Chem.* **1990**, *289*, 55. (c) Balasubramanian, T. S.; Vijayamohan, K.; Shukla, A. K. *J. Appl. Electrochem.* **1993**, *23*, 947.
- (3) Manohar, A.; Malkhandi, S.; Yang, B.; Yang, C.; Prakash, G. K.; Narayanan, S. R. *J. Electrochem. Soc.* **2012**, *159*, A1209.
- (4) (a) Ulman, A. *Chem. Rev.* **1996**, *96*, 1533. (b) Whitesides, G. M.; Laibinis, P. E. *Langmuir* **1990**, *6*, 87. (c) Schreiber, F. *Prog. Surf. Sci.* **2000**, *65*, 151. (d) Dubois, L. H.; Nuzzo, R. G. *Annu. Rev. Phys. Chem.* **1992**, *43*, 437. (e) Love, J. C.; Estroff, L. A.; Kriebel, J. K.; Nuzzo, R. G.; Whitesides, G. M. *Chem. Rev.* **2005**, *105*, 1103. (f) Bain, C. D.; Biebuyck, H. A.; Whitesides, G. M. *Langmuir* **1989**, *5*, 723.

(g) Troughton, E. B.; Bain, C. D.; Whitesides, G. M.; Nuzzo, R. G.; Allara, D. L.; Porter, M. D. *Langmuir* **1988**, *4*, 365. (h) Nuzzo, R. G.; Allara, D. L. *J. Am. Chem. Soc.* **1983**, *105*, 448143. (i) Porter, M. D.; Bright, T. B.; Allara, D. L.; Chidsey, C. E. D. *J. Am. Chem. Soc.* **1987**, *109*, 3559.

(5) (a) Yamamoto, Y.; Nishihara, H.; Aramaki, K. *J. Electrochem. Soc.* **1993**, *140*, 436. (b) Volmer-Uebing, M.; Reynders; Stratmann, M. *Werkst. Korros.* **1991**, *42*, 19. (c) Nozawa, K.; Nishihara, H.; Aramaki, K. *Corros. Sci.* **1997**, *39*, 1625. (d) Haneda, R.; Aramaki, K. *J. Electrochem. Soc.* **1998**, *145*, 1856. (e) Saleh, J. M.; Al-Haidari, Y. K. *Bull. Chem. Soc. Jpn.* **1989**, *62*, 1237. (f) Volmer-Uebing, M.; Stratmann, M. *Appl. Surf. Sci.* **1992**, *55*, 19. (g) Kong, D.-S.; Yuan, S.-L.; Sun, Y.-X.; Yu, Z.-Y. *Surf. Sci.* **2004**, *573*, 272. (h) Volmer, M.; Stratmann, M.; Viehhaus, H. *Surf. Interface Anal.* **1990**, *16*, 278. (i) Uehara, J.; Aramaki, K. *J. Electrochem. Soc.* **1991**, *138*, 3245. (j) Weber, C. R.; Dick, L. F. P.; Benítez, G.; Velab, M. E.; Salvarez, R. C. *Electrochim. Acta* **2009**, *54*, 4817. (k) Nozawa, K.; Aramaki, K. *Corros. Sci.* **1999**, *41*, 57. (l) Grundmeier, G.; Reinartz, C.; Rohwerder, M.; Stratmann, M. *Electrochim. Acta* **1998**, *43*, 165.

(6) (a) Swietnlow, A.; Skoogand, M.; Johansson, G. *Electroanalysis* **1992**, *4*, 921. (b) Schreiber, F. *Prog. Surf. Sci.* **2000**, *65*, 151. (c) Laibinis, P. E.; Whitesides, G. M.; Allara, L. D.; Tao, Y. T.; Parikh, A. N.; Atul, N.; Nuzzo, R. G. *J. Am. Chem. Soc.* **1991**, *113*, 7152. (d) Dubois, L. H.; Zegarski, B. R.; Nuzzo, R. G. *J. Chem. Phys.* **1993**, *98*, 678. (e) Nishi, N.; Hobara, D.; Yamamoto, M.; Kakiuchi, T. *J. Chem. Phys.* **2003**, *118*, 1904. (f) Park, B.; Chandross, M.; Stevens, M. J.; Grest, G. S. *Langmuir* **2003**, *19*, 9239. (g) Jennings, G. K.; Munro, J. C.; Yong, T.-H.; Laibinis, P. E. *Langmuir* **1998**, *14*, 6130. (h) Kawaguchi, T.; Yasuda, H.; Shimazu, K. *Langmuir* **2000**, *16*, 9830. (i) Dai, Z.; Ju, H. *Phys. Chem. Chem. Phys.* **2001**, *3*, 3769. (j) Porter, M. D.; Bright, T. B.; Allara, D. L.; Chidsey, C. E. D. *J. Am. Chem. Soc.* **1987**, *109*, 3559. (k) Bain, C. D.; Troughton, E. B.; Tao, Y.-T.; Evall, J.; Whitesides, G. M.; Nuzzo, R. G. *J. Am. Chem. Soc.* **1989**, *111*, 321. (l) Chen, S. H.; Frank, C. W. *Langmuir* **1989**, *5*, 978.

(7) (a) DeCarvalho, J.; Tremiliosi Filho, G.; Avaca, L. A.; Gonzaiez, E. R. *Int. J. Hydrogen Energy* **1989**, *14*, 161. (b) Cornell, A.; Lindbergh, G.; Simonsson, D. *Electrochim. Acta* **1992**, *37*, 1873. (c) Kreysa, G.; Håkansson, B. *J. Electroanal. Chem.* **1986**, *201*, 61.

(8) (a) Miller, C. J.; Cuendet, P.; Gratzel, M. *J. Phys. Chem.* **1991**, *95*, 877. (b) Finklea, H. O.; Snider, D. A.; Fedyk, J. *Langmuir* **1993**, *9*, 3660. (c) Chidsey, C. E. D. *Science* **1991**, *251*, 919.

(9) Atkinson, C. M. L.; Richardson, M. J. *Trans. Faraday Soc.* **1969**, *65*, 1749.

(10) (a) Rampi, M. A.; Schuller, O. J. A.; Whitesides, G. M. *Appl. Phys. Lett.* **1998**, *72*, 1781. (b) Clegg, R. S.; Hutchison, J. E. *J. Am. Chem. Soc.* **1999**, *121*, 5319. (c) Slowinski, K.; Chamberlain, R. V., II; Bilewicz, R.; Majda, M. *J. Am. Chem. Soc.* **1996**, *118*, 4709. (d) Slowinski, K.; Majda, J. *J. Electroanal. Chem.* **2000**, *491*, 139.

(11) (a) Friebel, S.; Aizenberg, J.; Abad, S.; Wiltzius, P. *Appl. Phys. Lett.* **2000**, *77*, 2406. (b) Huang, J.; Hemminger, J. C. *J. Am. Chem. Soc.* **1993**, *115*, 3342.